CHAPTER 16

GENERIC PERFORMANCE AND ENVIRONMENTAL ASSESSMENT OF A RADIOACTIVE WASTE REPOSITORY IN KOREA

Chang Lak Kim, Myung Chan Lee and Jang Soo Nam

Nuclear Environment Management Center, Taejon, Korea

Abstract. The Nuclear Environment Management Center (NEMAC), a subsidiary of the Korea Atomic Energy Research Institute (KAERI), has conducted a performance and environmental assessment of the proposed Korean radioactive waste repository. In this paper, a description is provided of the performance and environmental assessment of a generic Korean radioactive waste repository.Adescription is given of the various data needed in post-closure performance assessment calculations. The data are divided into four major categories: inventory and design data, chemical data, hydrogeological data, and biosphere data. The results suggest that a generic performance assessment of the conceptual repository may be acceptable when measured against the regulatory criteria. The results indicate, however, that the performance will be strongly dependent on the geology and hydrogeology of the repository location, and it should be noted that the assessment was carried out on the basis of a limited understanding of the site-specific characteristics. It will be necessary to obtain site-specific data at the intended repository location in order to enable a more detailed assessment to be undertaken. This preliminary assessment of the conceptual repository provides a firm foundation for future site-specific assessment activities.

16.1 INTRODUCTION

The radioactive waste management program in Korea dates back to mid-eighties when KAERI perceived, from prior studies, the necessity for a national program for a comprehensive and systematic management of radioactive wastes including spent fuel arising from this country's ambitious nuclear power plant program. The recommendation therefrom was taken in consideration by the Korea Atomic Energy Commission which made a decision at its 221st meeting in 1988 to establish a relevant program to be implemented. Institutional arrangement for this program was that the required waste fund be levied on waste generators by the "polluter pays" principle. Initial works of the program had been implemented, including conceptual design of a low-level radioactive waste repository and the development of transport casks, until the whole program has been seriously hindered by the difficulty of site acquisition.

The major difficulty in site acquisition came from opposition of local communities at potential sites. The bad image of waste burial, combined with fear of potential nuclear danger, seems to have made the local communities abhorrent to any attempt to access the sites as culminated by the Anmyon Island incident in late 1990, where a series of demonstrations by local residents influenced the government to cancel the nomination of the site. All the efforts of NEMAC and the government to convince the local communities of potential sites have failed in a social mood overwhelmed by the NIMBY syndrome and an anti-nuclear movement. At the end of 1994, the government nominated Guleop Island, with only nine residents, as the candidate site for the repository and later finalized it as the official site. However, even after the governmental announcement, a series of demonstrations by the residents of Dukjuk Island, mother island of the smaller Guleop Island, acted as big obstacle against the government and NEMAC. The final blow against the Guleop Island Project was made at the end of 1995 by the confirmation of active fault zones, near and on the island, so that the government had to announce the cancellation. After a decade of unsuccessful efforts in search of a site, the government decided to amend the institutional approach to the problem.

In this paper, the groundwater pathway results of a performance and environmental assessment study[1] of the

conceptual Korean radioactive waste repository, carried out jointly by NEMAC and AEATechnology from 1994 to 1995, are summarized.

In Section 16.2, a description is given of various data used in the assessment calculations. In Section 16.3, a description is given of the assessment calculations undertaken to address radionuclide transport along the groundwater pathway; this was the major component of the post-closure performance assessment. However, the results of the assessment carried out to address the effects of gas generation and migration on the performance of the proposed Korean repository and the calculations carried out to address the radiological risks arising from inadvertent human intrusion into the proposed repository are not included in this paper.

16.2 PREPARATION OF ASSESSMENT DATA

16.2.1 Design and Inventory Data

Radioactive wastes requiring treatment and disposal in Korea are dominantly produced by operation of the civil nuclear power reactors. These are of the PWR and CANDU types, and produce a range of wastes in the low- and intermediate-level categories. Spent fuel is not considered at this time.

The levels of radioactive contamination vary widely, and a proportion of each of the first three waste types appears in both the LLW and ILW categories. The choice of waste treatment technologies reflects this variation.

The liquid concentrates come from the treatment of water discharged from the primary reactor circuit, the secondary heat transfer circuit, and the spent fuel storage pools. The water is treated so that dissolved contaminants are precipitated, and it is then evaporated to reduce the volume. Using current technology, the resulting 'sludge' is mixed directly with cement and poured into 200-litre disposal drums. In the near future, material may be evaporated to dryness and disposed in drums containing a paraffin wax encapsulation matrix.

The ion exchange resins arise from in-service clean-up of the water circuits and spent fuel pool. When they have served their useful life, they are discharged and treated for disposal. Using the current technology, resins are cemented directly into 200-litre drums. In the future, resins will be dried and loaded into high-integrity containers (HIC), composed of stainless steel, which will be welded shut.

The spent filters arise from various air and water filtration uses around the power plants. Some of them are of the HEPA type and consist largely of paper. All filters are treated in the same manner, by direct cementation into 200 litre drums.

General contaminated trash arises from day-to-day operations at the power plants, and consists of contact clothing, wipes, sample containers, redundant equipment and tools, etc. Some of this material may not be contaminated at all, but the general policy is to prevent accidental spread of contamination by treating all waste from the active area as if it were radioactive. These wastes will be loaded into 200 litre drums, and subjected to high-force compaction, reducing their volume by a factor of three or more. The resulting 'pucks'will then be loaded into larger overpack drums (of about 300 litre capacity) for disposal.

Korean repository design

The conceptual design of Korean repository[2] (for the initial phase of the repository construction) consists of the following five caverns, as illustrated in Figure 16.1:

a. LLW (Type I) cavern;
b. LLW (Type II) caverns (two caverns);
c. LLW (Type III) cavern; and
d. ILW cavern.

The cross-sectional designs of the LLW and ILW caverns are illustrated in Figures 16.2 and 16.3, respectively. Physical parameters defining the cavern and disposed waste volumes are given in Table 16.1.

It should be noted that no decision has yet been made concerning the backfilling strategy to be adopted in the ILW cavern. The implications for repository performance of various backfilling strategies for the ILW cavern were addressed in this performance assessment. These strategies consist of:

a. cementitious backfill;
b. 10% bentonite / 90% crushed rock mixture; and
c. no backfill.

Waste inventory

Summary information for each of the radionuclides

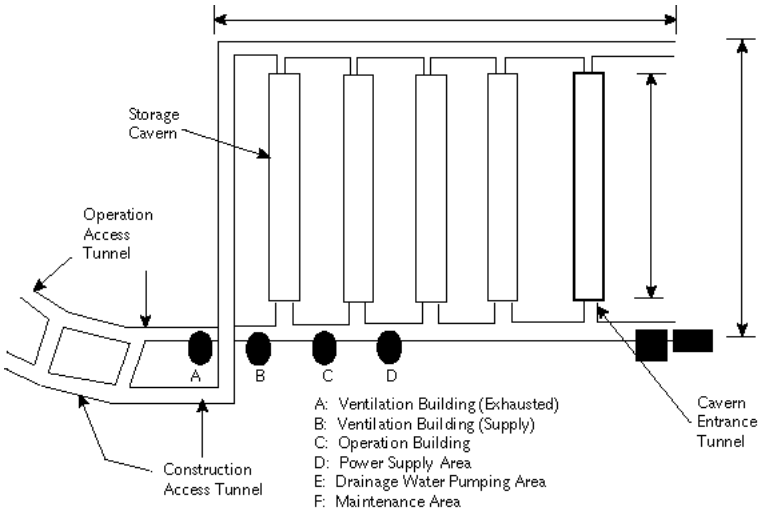

Figure 16.1. Proposed layout of Korean repository (Initial Phase).

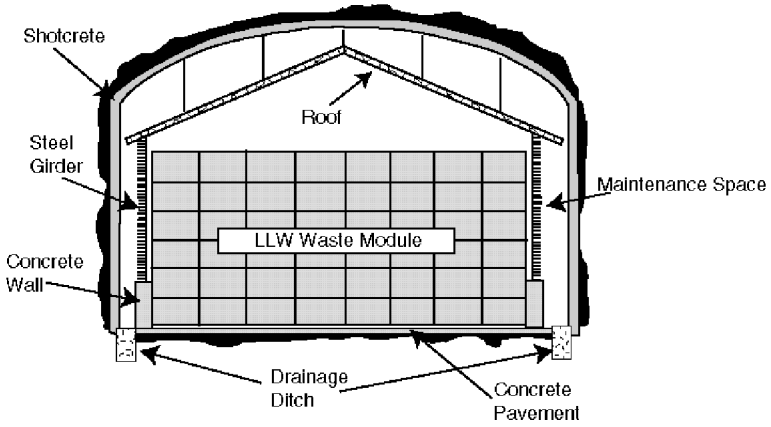

Figure 16.2. Cross section of LLW cavern.

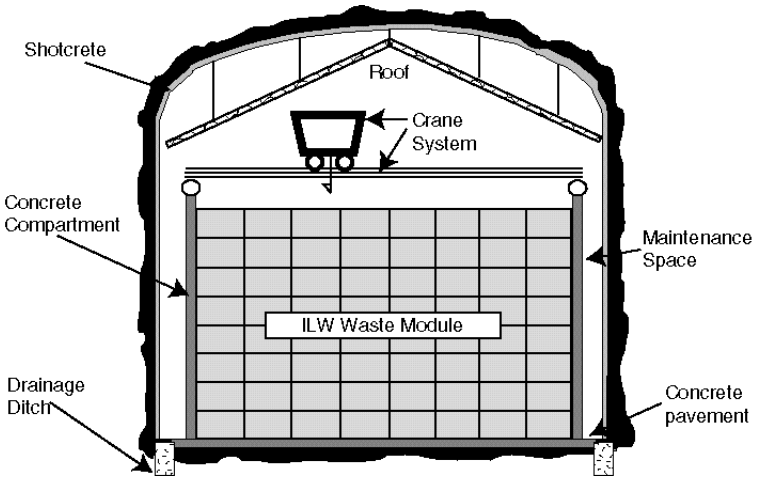

Figure 16.3. Cross section of ILW cavern.

Table 16.1. Cavern and disposed waste volumes (m^3).

Parameter	LLW (Type I)	LLW (Type II) (total)	LLW (Type III)	ILW
V_{wst}(a)	$3.85\ 10^3$	$7.26\ 10^3$	$3.37\ 10^3$	$5.52\ 10^3$
V_{dmod}(b)	$1.08\ 10^4$	$2.15\ 10^4$	$1.08\ 10^4$	$1.49\ 10^4$
$V_{b/f}$(c)	-	-	-	$3.05\ 10^4$
V_{exc}(d)	$2.73\ 10^4$	$6.06\ 10^4$	$3.03\ 10^4$	$5.62\ 10^4$

Notes:
(a) Volume of packaged waste in 200 litre containers.
(b) Volume of disposal module (6-pack LLW) or 8-pack (ILW).
(c) Volume of backfill (ILWonly).
(d) Total volume of caverns.

appears in Table 16.2. A summary of the number of drums in each cavern associated with each waste type and of the total volume occupied by the wasteform is provided in Table 16.3.

16.2.2 Chemical Data

Calculations have been carried out to investigate the chemistry of the JWS-2 groundwater, collected at a depth of 330 m, which was considered to have a chemistry most analogous to that in the vicinity of the study area. The aqueous speciation of this groundwater and the likelihood of certain minerals precipitating or dissolving has been modelled using the HARPHRQ program[3] with the HATCHES database[4]. Further calculations have been performed to predict the effect of groundwater equilibration with a high-calcium cement. These calculations have been used as the basis for determining the solubility of a number of key radionuclides in two groundwaters, the JWS-2 water at pH 5.7 and a cement-equilibrated water at pH 12.9.

The PDFs for elemental solubility limits that were used in this assessment were centred on the results of the HARPHRQ speciation calculations, with log-triangular PDFs covering whole orders of magnitude. The main materials of interest to the conceptual repository are the in-drum cement, concrete and bentonite (candidate backfill materials for the ILW caverns), and the mineral andesite, which is the host rock considered for this study.

Table 16.2. Radionuclide Inventory.

Radionuclide	Half-life (years)	Inventory (Bq)
^{3}H	$1.24\ 10^1$	$4.31\ 10^{12}$
^{14}C	$5.73\ 10^3$	$4.11\ 10^{12}$
^{60}Co	$5.27\ 10^0$	$6.16\ 10^{14}$
^{59}Ni	$7.50\ 10^4$	$1.02\ 10^{13}$
^{63}Ni	$9.60\ 10^1$	$3.12\ 10^{14}$
^{90}Sr	$2.91\ 10^1$	$7.95\ 10^{12}$
^{94}Nb	$2.03\ 10^4$	$2.46\ 10^{11}$
^{99}Tc	$2.13\ 10^5$	$3.34\ 10^{11}$
^{129}I	$1.57\ 10^7$	$1.93\ 10^{10}$
^{137}Cs	$3.00\ 10^1$	$3.41\ 10^{14}$
^{235}U	$7.04\ 10^8$	$1.11\ 10^7$
^{238}U	$4.47\ 10^9$	$3.91\ 10^8$
^{238}Pu	$8.77\ 10^1$	$1.59\ 10^{11}$
^{239}Pu	$2.41\ 10^4$	$3.28\ 10^{11}$

Table 16.3. Waste inventory.

Waste type	Number of drums	Volume occupied (m^3)			
		LLW (Type I)	LLW (Type II)	LLW (Type III)	ILW
Liquid conc. in cement	10,425	-	4,996	-	$3.08\ 10^3$
Liquid conc. in paraffin	-	-	-	10,273	$2.05\ 10^3$
Ion exchange resin in cement	4,516	-	-	-	$9.03\ 10^2$
Ion exchange resin in HIC	-	-	-	16,445	3.2910^3
Spent filters in cement	4,307	-	-	882	1.0410^3
General trash	-	36,288	11,868	-	$9.63\ 10^3$

Aliterature survey has been carried out to determine the likely Rd values for sorption of radionuclides onto the bentonite backfill and onto the host rock formation.

16.2.3 Hydrogeological Data

The first step in the development of a numerical model of the groundwater flow in the region around the study area is to develop a conceptual model of the geological and hydrogeological structure of the region. The general direction of groundwater flow in the region around the hypothetical repository location would be from the high ground inland towards, and roughly perpendicular to the coast. The most appropriate type of model to construct for this illustrative assessment was therefore a two-dimensional vertical cross-section model along a line roughly perpendicular to the coast. It was noted that the model would have to extend some distance offshore so that the saline transition zone near the coast could be modelled satisfactorily. The geological structure along the main line of section selected for the groundwater flow model is shown in Figure 16.4.

In order to carry out this preliminary assessment, input PDFs were required for all of the hydrogeological properties used in the groundwater flow and transport models. The materials identified in the geological structure were:

1. upper andesite;
2. lower andesite;
3. fractured lower andesite;
4. granite;
5. shale;
6. sandstone/mudstone/siltstone sediments; and
7. gneiss.

In addition, the hydrogeological properties of the repository itself, and of the access tunnels, had to be considered. A PDF was required for the permeability and porosity of the material in three cases: normal rock, rock within a fault core, and rock within a fault halo. The notation T(a,b,c) is used to indicate a triangular PDF with upper and lower limits c and a, respectively, and peak value b. For convenience, logarithms to base 10 were used. The hydraulic conductivity for some of the rock types are summarized in Table 16.4, as an example.

16.2.4 Biosphere Data

The approach adopted is to identify critical groups, and hence to evaluate potential maximum individual risks. This evaluation is based on the definition of hypothetical subsistence communities, which are assumed to make maximum reasonable use of local food resources and to be located in the area of the environment assessed to be the most contaminated as a result of possible future discharges from the repository.

In this assessment, the screening process was carried out using the generic biosphere program BIOS_3A[5], which considers a relatively wide range of potentially important pathways. On the basis of the screening calculations, a simple process model was developed taking advantage of the Compartment Biosphere submodel available within the MASCOT program[6].

The terrestrial biosphere considered comprises the

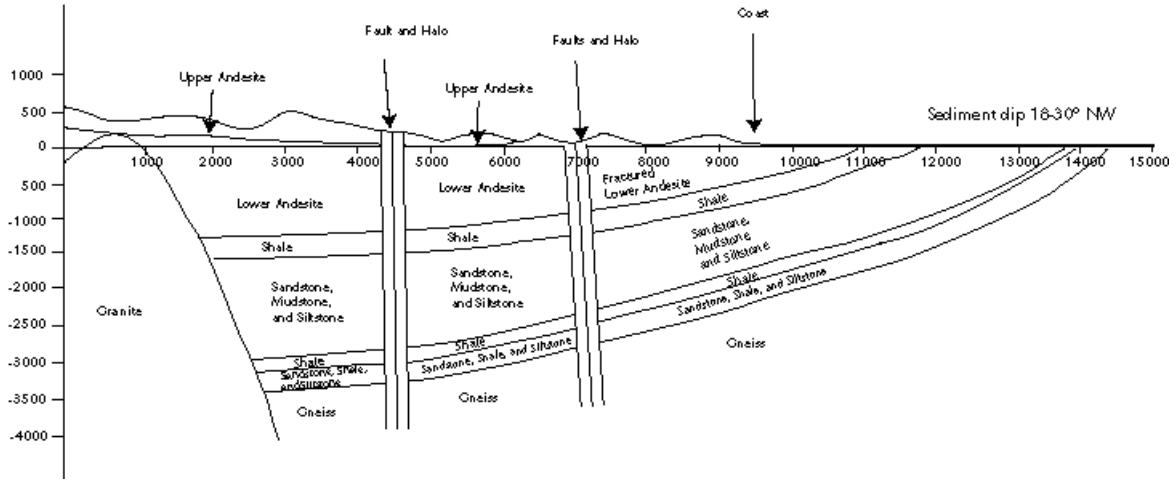

Figure 16.4. Geological structure along the line of the model cross section. Distances and elevations in metres.

Table 16.4. Summary of log-hydraulic conductivity distributions.

Rock type	Log-hydraulic conductivity[(a)]			Comment
	Lower bound	Peak	Upper bound	
Andesite	-12	-8	-6	Isotropic
Fractured Andessite	-11	-7	-5	Isotropic
Granite	-11	-8	-6	Isotropic
Gneiss	-13	-10	-7	Isotropic
Shale	-12	-9	-7	Isotropic
Sandstones	-10	-7.6	-5	Isotropic

Note: (a) Values given are for log-hydraulic conductivity (permeabilities in m s^{-1}, log to base 10).

catchment of a small river discharging into a coastal sea. The section of river that may be contaminated by groundwater from the repository, either directly or indirectly (through drainage from adjacent farmland), is estimated to be 5 km in length, and the area of its associated catchment, 10 km^2.

The critical group at risk from radionuclides entering the biosphere is assumed to be a community of subsistence farmers who live and work in the land. For the preliminary assessment, their diet was assumed to be similar to the Korean average.

The endpoint of the calculations corresponds to the maximum dose received resulting from a steady 1 Bq yr^{-1} release rate from the geosphere, which occurs as concentrations in the environment approach, steady-state equilibrium values. The calculations demonstrated that a wide range of terrestrial pathways should be considered. Marine pathways, however, were found to be less important, because of much higher levels of dilution in coastal waters. The results of the analysis using BIOS_3A provided a basis for selecting pathways for the second phase of the assessment using MASCOT's biosphere compartment submodel facility. Terrestrial pathways considered in the second stage of the assessment using MASCOT included ingestion of rice and vegetables, drinking water, consumption of meat products (beef, milk, liver, and poultry), external gamma exposure from soil, and dust inhalation. Although less important, ingestion of marine foodstuffs was also considered.

Figure 16.5 shows the structure of the biosphere model developed for the preliminary assessment.

16.3 GROUNDWATER PATHWAY

16.3.1 Groundwater Flow Modelling

After the closure and resaturation of a repository for radioactive waste, it can be anticipated that radionuclides will dissolve in groundwater flowing through the wasteform and will be transported with the groundwater through the geosphere to the biosphere. This is the natural pathway by which radionuclides, disposed in a repository, may return to the human environment. It is almost certain that radionuclides will return to the bios-

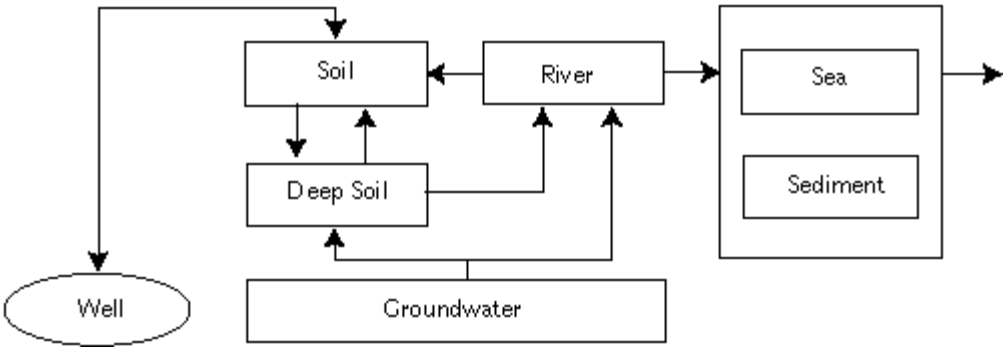

Figure 16.5. Structure of biosphere model.

Figure 16.6. Shade plot of the NAMMU patch grid showing assignment of rock types. The lines from the repository locations represent the access tunnels.

phere by this route, and so an analysis of the risk arising from the groundwater pathway forms an important part of an assessment of the performance of a repository for radioactive waste.

In order to carry out this analysis, it is necessary to be able to estimate the rate of groundwater flow in the vicinity of the repository (which largely determines the flux of radionuclides leaving the repository) and the nature of the regional groundwater flow system (which determines the subsequent transport through the geosphere and return to the biosphere).

The first stage in the development of a NAMMU groundwater flow model[7] of the site is the construction of a finite-element mesh that represents the important features of the geology and topography of the site (see Fig. 16.4) and extends to regions where well-defined boundary conditions can be identified. Careful design of the finite-element mesh is necessary both to ensure that the numerical solution is as accurate as possible and to allow for subsequent changes to the model to be made with ease.

The top surface of the mesh was a smoothed representation of the topography, treated as a number of straight-line segments that preserved the major features. The left-hand boundary of the model was taken to be an assumed (vertical) groundwater divide under the high ground inland.

The gneiss has a very low permeability and so, in principle, the base of the sediments could have been taken to form the base of the model. However, a satisfactory treatment of the region of saline groundwater offshore would require that the distribution of salt concentration on the base of the sediments be known a priori, which is not the case. It was therefore preferable that the model extended far enough offshore to include the offshore surface outcrop of the gneiss. It is then reasonable to assign a constant salt concentration along the right-hand boundary of the model. Figure 16.6 shows the assignment of rock types in the base-case model. The aim was to produce a grid in which the largest elements were about 200-250 m across. In practice most of the elements are considerably smaller. The final grid used for the calculations is shown in Figure 16.7.

The overall (large-scale) flow is driven by the high heads produced by the high ground on the left-hand side of the model and moves downwards towards the right-hand side of the model. This flow continues at depth until it reaches the salt front, which is intruding from the right-hand side of the model. The saline transition zone is at the point where the driving head from the topography exactly balances the head due to the increased density of the seawater. The freshwater therefore flows up the salt front and discharges near the coast. Seawater intrudes from the right-hand boundary of the model and flows into the model until it reaches the saline transition zone, which it flows up before discharging through the sea bed. In the near-surface part of the model onshore, small flow cells driven by local topographic variations are superimposed on the large-scale flow. Local discharge occurs in all of the small valleys represented in the model. There is very little flow in the gneiss layer.

A series of pathline calculations were performed to investigate the general nature of the flow system. The pathlines that were used for the MASCOTanalysis were started from the following two sets of points: (3600,55), (3700,55), and (3800,55) to represent paths starting from the ‘upper repository’(i.e. a repository located 50 m above OD, about 250 m below the ground surface),

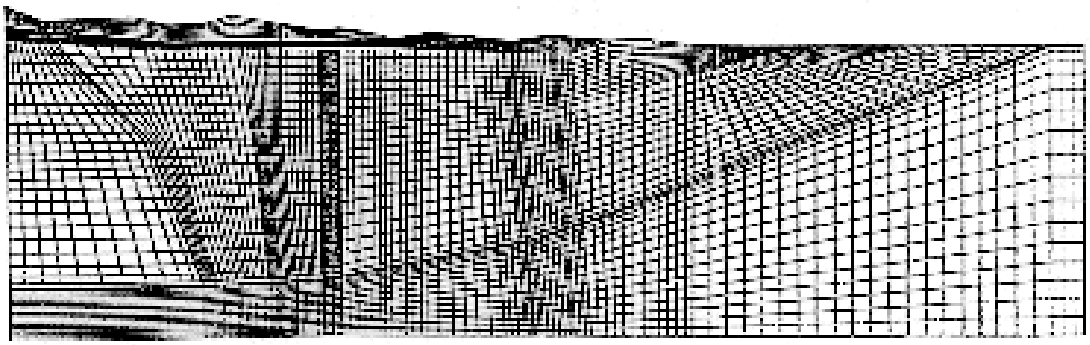

Figure 16.7. Plot of finite-element mesh.

and (3600, - 50), (3700, - 50), (3800, - 50) to represent pathlines starting from the 'lower repository' (i.e. a repository located 50 m below OD, about 350 m below the ground surface). The travel times and path lengths for these paths, and the specific discharges at the repository locations, are summarized in Table 16.5.

One of the pathlines that was started from the upper repository position crossed the fault zone near the repository and emerged near the tunnel entrance after a travel time of approximately 1200 years. The other two pathlines from the upper repository position emerged up the fault zone with travel times of approximately 500 years after being caught in the flow cell that discharges in the small valley near the fault (Fig. 16.8a). All three pathlines that started from the lower repository crossed the fault and emerged near the tunnel entrance with travel times of about 1100 years (Fig. 16.8b). Three pathlines were also started from a location near the coast, solely in order to illustrate the general nature of the flow in the vicinity of a hypothetical repository sited there. Two of the pathlines emerged a short distance offshore, but the third was caught in a local flow cell and emerged in the valley closest to the coast (see Fig.16.8c).

Finally, a calculation was performed to estimate the resaturation time of the repository. The base-case model was modified to apply a boundary condition of atmospheric pressure at the repository location. The total flow of groundwater into the repository induced by this condition was then estimated by integrating the specific discharge along the four sides of a box closely matching the repository location, and then multiplying the result by the width of the repository perpendicular to the cross section. The resaturation time is then estimated by dividing the empty volume of the repository by the volume of flow towards the repository.

The total flow into the repository in the two-dimensional model was found to be $4.67\ 10^{-6}$ m^2s^{-1}. The reposito-

Table 16.5. Results of the base-case pathline calculation.

(a) Upper Repository

Path	Travel time (years)	Pathlength (m)	Repository specific discharge (x component, m s^{-1})	Repository specific discharge (y component, m s^{-1})
1	1176.2	1828.6	$1.2265\ 10^{-9}$	$-8.684\ 10^{-10}$
2	565.93	971.61	$1.3302\ 10^{-9}$	$-6.9320\ 10^{-10}$
3	432.12	777.98	$1.3916\ 10^{-9}$	$-5.1647\ 10^{-10}$

(b) Lower Repository

Path	Travel time (years)	Pathlength (m)	Repository specific discharge (*x* component, m s^{-1})	Repository specific discharge (*y* component, m s^{-1})
1	1243.1	1882.9	$1.0702\ 10^{-9}$	$-7.4150\ 10^{-10}$
2	1114.8	1722.3	$1.1650\ 10^{-9}$	$-6.0711\ 10^{-10}$
3	1049.1	1602.4	$1.2276\ 10^{-9}$	-4.684510^{-10}

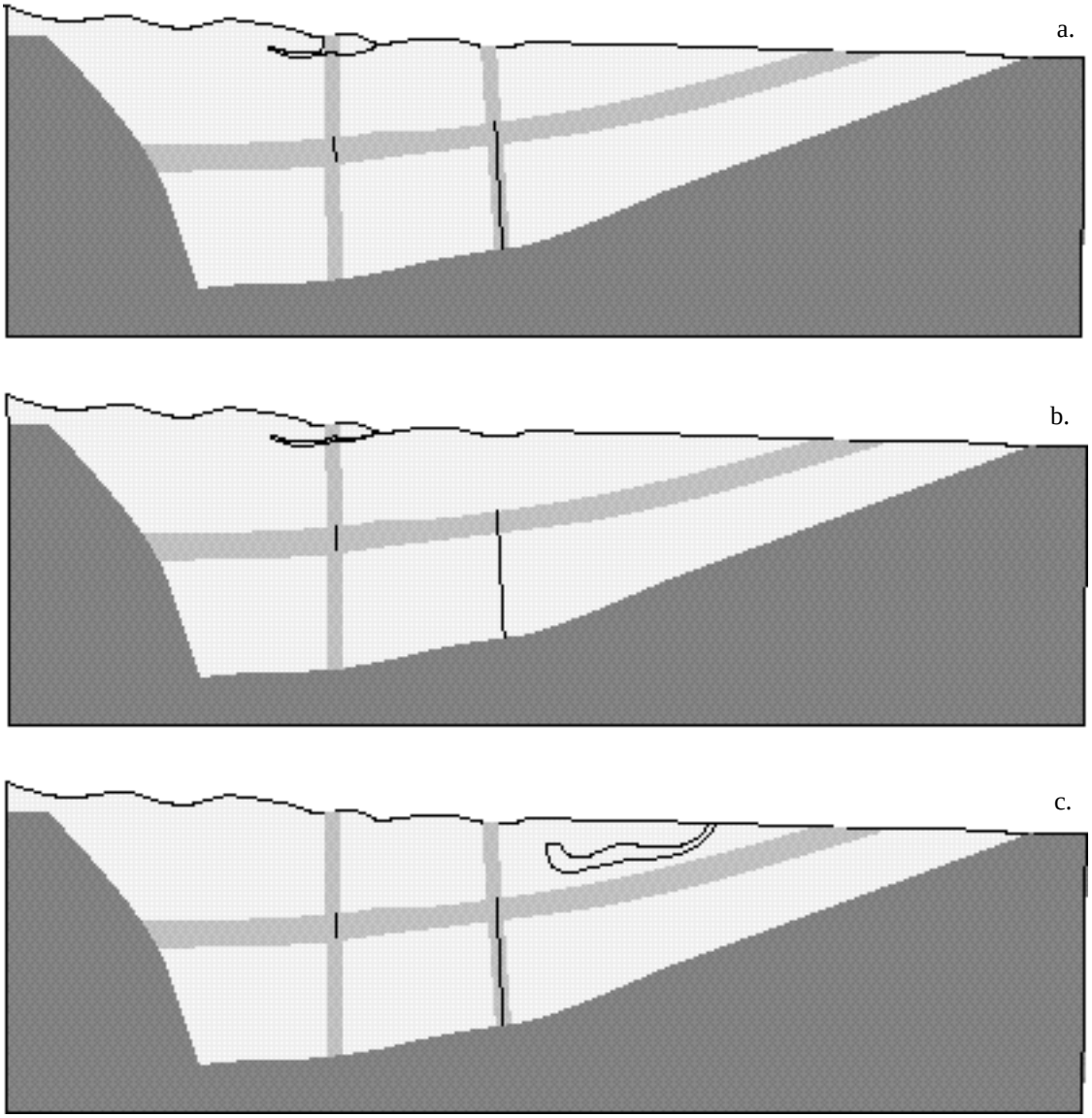

Figure 16.8. Results for some key pathlines: a - From the upper repository position; b - From the lower repository position, and c - From the coastal repository position.

ry region was taken to have a length of 440 m perpendicular to the section, giving a total flow into the repository region of 2.05 10^{-3} m^3s^{-1}. The total empty volume of the caverns after repository closure is 1.54 10^5 m^3, which gives a resaturation time of 2.4 years. This short time is a result of the high heads above the repository location and the relatively high permeability of the andesite. It should be noted that as the repository resaturates, its pressure will rise and the inflow will be correspondingly reduced. Thus, the value given above is likely to be an underestimate of the resaturation time.

16.3.2 System Model for Groundwater Pathway

In this subsection, the construction of an overall model of the system for groundwater-mediated return of radionuclides to the biosphere is explained.

Source-term submodels

The repository under consideration is planned to contain wastes of several different types, and there will be some degree of segregation into different parts of the repository. The different waste types can therefore be expected to contribute differently to the source term. In general, the key factors determining source-term behaviour

Table 16.6. Calculated buffering times for caverns.

Cavern	Amount of CaO (mol m^{-3})	Buffering time at pH12.2 (yr)
LLW (Type I)	975	$1.5\ 10^3$
LLW II	0	0.0
LLW III	218	$3.3\ 10^2$
ILW (no backfill)	20	$3.2\ 10^1$
ILW (bentonite backfill)	20	$3.8\ 10^4$
ILW (concrete backfill	2,400	$4.6\ 10^6$

are:

a. degradation of the physical containment;
b. chemical control on the solution concentration of the radionuclides; and
c. the rate of groundwater flow through the repository.

Although physical containment of the wastes is important during the operational phase of the repository, the long-term behaviour after closure will be affected significantly by physical containment only in the case of containers specially engineered for exceptional performance. It is recommended that for all wastes in 200 - litre mild steel drums, physical containment be ignored, since all the other time scales involved in release and transport of radionuclides will be much longer than the expected corrosion lifetime of these drums. For the ion exchange resins in stainless steel HIC containers, however, a period of absolute containment should be modelled.

Some of the source term models selected for analysis of the release of radionuclides take account of the conditioning of the pore water to high pH by dissolution of free calcium hydroxide in the cements. It is appropriate to analyse each disposal vault, to determine whether there is sufficient $Ca(OH)_2$ to buffer the pH during the relevant assessment period.

The results of a simple analysis are given in Table 16.6 for each type of disposal vault; note that the buffering times are averaged across the entire vault, and do not represent the smaller-scale buffering within packages. This analysis indicates that the current plans would result in a wide range of buffering times for the various vaults. The LLW I and backfilled ILW vaults would clearly be buffered for a substantial length of time, whereas the LLW II and non-backfilled ILW vaults would not. The LLW III vaults represent an intermediate case. It is clear that extended buffering of pore water to high pH would require either increased amounts of free $Ca(OH)_2$, or reduced groundwater flow through the vaults (most easily achieved by backfilling).

Because the six types of waste are distributed in different caverns, it was necessary to adopt an approach in which nine different source-term submodels were used, as shown in Figure 16.9.

The submodels LLW1A, LLW1B, etc. are MASCOT Containment submodels, which are used to specify the initial inventory of each radionuclide, and any time of absolute containment of the waste. These feed into source-term submodels, ST1A, ST1B, etc., which calculate the release of the radionuclides. The purpose of each of these submodels is summarized in Table 16.7.

In Figure 16.9, the submodels named DIST1 and DIST2 are Distributor submodels used in MASCOT for combining and/or redistributing fluxes between submodels. In this case, DIST1 adds the outputs of the three ILW source-term submodels to provide the input to submodel BARR, which represents the barrier provided by the backfill in the ILWcavern. Finally, DIST2 adds the output of BARR and those of all the LLW caverns to make the total source-term output to be fed into the Geosphere section of the system model.

The BARR submodel is added to represent the time delay for release of radionuclides from the ILW cavern into the geosphere, arising because of the backfill in that cavern. For initial calculations, it was decided to treat the effect by using a porous geosphere submodel, with nominal water transit time equal to the approximate time for water molecules to diffuse through the barrier. The different radionuclides would then be transported through this barrier submodel in times longer than this, according to their retardation coefficients, calculated from sorption distribution coefficients appropriate to the backfill material.

Geosphere transport submodels

From the pathline calculations, two possible pathways

Table 16.7. Source-term submodels within MASCOT system model.

Name	Submodel type	Representing
ST1A	SLST[(a)]	Cemented liquid concentrates (LLW cavern Type I)
ST1B	SLST[(a)]	Cemented ion-exchange resins (LLW cavern Type I)
ST1C	SLST[(a)]	Cemented filters (LLW cavern Type I)
ST2	SLST[(a)]	Compacted trash (LLW cavern Type II)
ST3A	SLST[(a)]	Cemented liquid concentrates (LLW cavern Type III)
ST3B	SLST[(a)]	Compacted trash (LLW cavern Type III)
ST4A	Leaching	Paraffin-encapsulated liquid concentrates (ILW cavern)
ST4B	Leaching	Ion- exchange resins in HIC (ILW cavern)
ST4C	SLST[(a)]	Cemented filters (ILW cavern)

Notes: (a) Solubility-limited source term.

from the repository to the surface emerged; the first (Path A) spending time in the upper/lower andesite, followed by a time crossing the fault zone, followed by a further time in the upper/lower andesite, the second (Path B) spending time in the upper/lower andesite followed by a time travelling vertically up the fault zone to the surface.

The network of geosphere submodels is shown in Figure 16.9. The input to the geosphere network is a combined flux from all the source terms (from submodel DIST2. The distributor submodel DIST3, divides the flux leaving the AND1AB submodel (representing the first section of andesite that occurs in both paths) into two parts, one which takes Path A (to submodel FAULTA), and one which takes Path B (to submodel FAULTB). The fluxes from the two paths are recombined in submodel DIST4 to provide a total flux to the biosphere. The

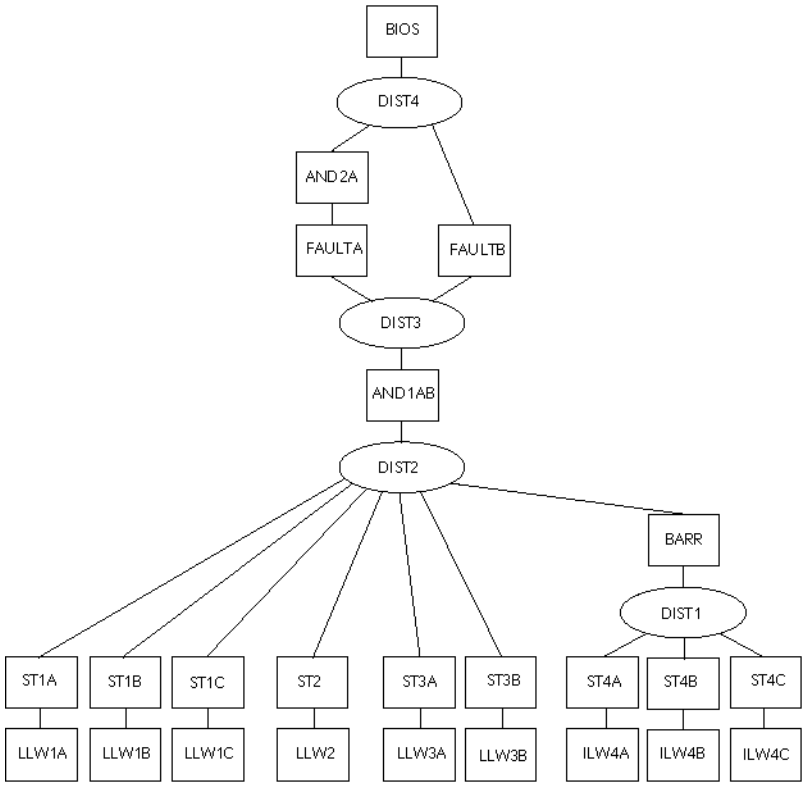

Figure 16.9. System model made up out of source term, geosphere, and biosphere submodels.

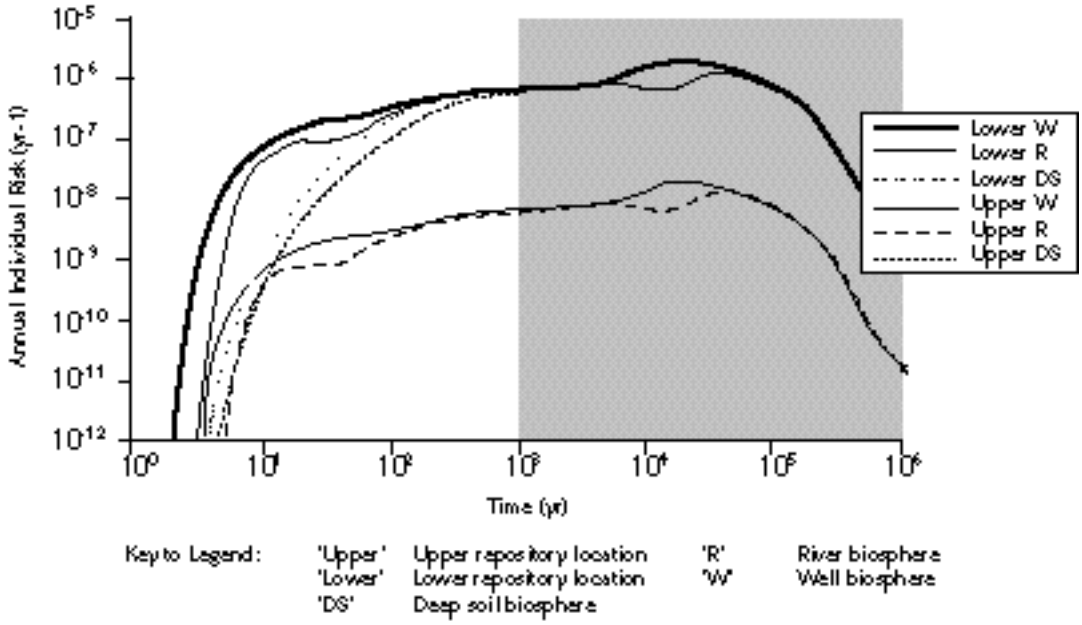

Figure 16.10. Total annual individual risk as a function of time for the upper and lower repository locations for each biosphere.

geosphere submodels represent the following:

AND1AB The first section of upper/lower andesite in which both paths Aand B spend time;
FAULTA Path Ain the fault zone;
FAULTB Path B in the fault zone to the surface;
AND2A Path A in the second section of upper/lower andesite to the surface.

All these submodels are MASCOT Porous Geosphere submodels. This type of submodel assumes that the rock matrix is fully accessed and hence the porosity is the full matrix porosity.

Biosphere submodels

Three exposure pathways were considered, in which the flux from the geosphere is released to the deep soil, a river and a well. Three identical compartment biosphere submodels (DEEPSOIL, RIVER and WELL) were used in MASCOT to represent the three exposure pathways, each taking as its input the entire flux from the geosphere. The difference between the three submodels was that the inlet was to different compartments appropriate to the three exposure pathways. The compartment structure of the biosphere is shown in Figure 16.5. The outlet from the biosphere was in each case a total dose from concentrations in soil, water (river or irrigation) and seawater.

16.3.3 Results

The total annual individual risks calculated for each biosphere model for the upper and lower repository locations are shown as functions of time in Figure 16.10. It can be seen that for both locations, the deep soil and well biospheres give very similar peak risks (marginally higher in the case of the well), whereas the river biosphere gives risks which are about two orders of magnitude lower.

The risk values, being obtained from mean doses that are estimated from a finite number of realizations (1000 for these runs), are subject to statistical error. From the variance of the observed values, this error can be estimated, and typical 95% confidence intervals are shown in Figure 16.11 (for the lower repository location). For most of the time-range, the upper 95% confidence limit exceeds the best estimate by a factor of about 1.5 or less. This is considered perfectly adequate for a preliminary assessment, with many uncertainties in the data and in the model choices that may well cause biases of rather greater magnitude. The statistical estimation errors could be reduced by including more realizations; to halve the error, four times the number of realizations would be necessary.

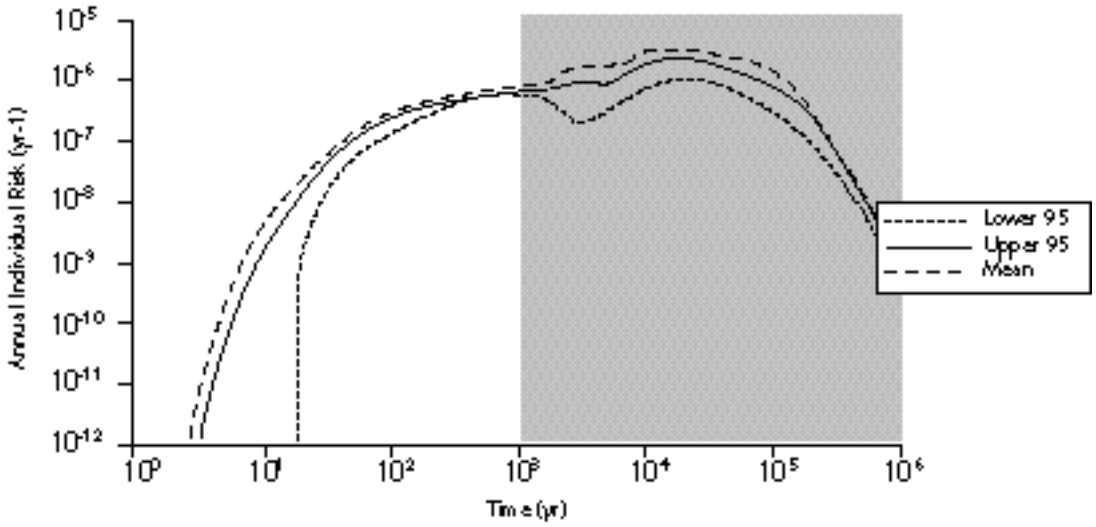

Figure 16.11. Total annual individual risk for release to the deep soil biosphere for the lower repository location plotted against time (with 95% confidence limits).

16.3.4 Discussion

Risk levels

Using the models and data adopted for these assessment calculations, it was found, for both choices of repository location and for all the alternative assumptions about the release point to the biosphere, that the predicted risk remained below the target of 10^{-6} yr^{-1} throughout the period of detailed quantitative assessment, up to 1000 years after closure. Beyond this time, no dramatic increases in risk were found, the greatest calculated mean risk being 1.4 10^{-6} between 10^4 and 10^5 years post-closure.

Because of the parameter-value uncertainties, which the probabilistic approach is designed to treat, different sampled realizations of the system gave conditional risks either higher or lower than the mean. From the calculated distributions, it was found that there was a probability of 0.25 to 0.30 of exceeding a risk of 10^{-6} for times up to 10^3 years, and a probability of about 0.50 of exceeding a risk of 10^{-6} for times up to 10^6 years.

Important radionuclides

Up to 1000 years after closure, only ^{129}I makes a significant contribution to risk, other radionuclides either being effectively contained, or else delayed in their passage through the geosphere. Beyond the 1000-year period, the only significant additional contributor to risk was found to be ^{59}Ni.

Effects of the alternative biosphere models

The risk curve for ^{129}I when using the biosphere model in which discharge to the deep soil is assumed, shows a substantially greater initial delay relative to that found using the river or well biosphere models. This suggests that the transport process (when present) from the deep soil to the other compartments provides a non-negligible supplement to the geosphere travel times. Apart from this difference, the shapes of the risk versus time curves for the three biosphere models are very similar.

Differences between the upper and lower repository locations

The peak risk for the upper repository location was found to be 9.8 10^{-7} for the deep soil biosphere and is due to ^{59}Ni. The ^{59}Ni curve clearly shows the difference between paths A and B as two separate peaks. For the lower repository location, the peak risk is higher, at 1.4 10^{-6} for the deep soil biosphere. In fact, the travel times are in general longer from the lower repository location. However, in this case the two peaks arising from paths A and B are not so obviously separated. For the lower repository location, the travel times for the total Path A and the total Path B are more comparable than they are for the upper repository location, and the reason that the risk is lower in the case of the upper location is that the larger difference between paths A and B causes more spreading to occur in the geosphere and hence reduces the risk. This interesting result shows that the spreading of arrival of radionuclides at the surface is not just a

matter of hydrodynamic dispersion, but can be contributed to by division of the transport between major alternative paths. However, it should be noted that these two calculations provide insufficient evidence to draw general conclusions about the relationship between repository placement and the extent of this type of dispersion.

Effect of parameter uncertainties

Whereas the expected contribution to risk from ^{59}Ni arises from just a small number of realizations that lead to relatively high conditional risks (those in which both the geosphere travel time and retardation of Ni are low), the contribution to risk from ^{129}I arises from a moderate risk in almost all realizations. This shows that the potential contribution to risk from ^{59}Ni could be subject to significant revision as future reductions are achieved in the present uncertainty about hydrogeological conditions and the retardation of Ni in the geosphere.

16.4 SUMMARY OF PROBABILISTIC SAFETY ASSESSMENT

Anumber of deterministic variant calculations were carried out, to explore the sensitivity of the system performance to several hypothetical changes. The changes addressed were:

a. no backfill in the ILW caverns;
b. concrete backfill in the ILW caverns;
c. high specific discharge at the source;
d. reduced geosphere travel times;
e. combination of (c) and (d); and
f. low near-field sorption coefficients.

These variations were considered relative to a base case defined by giving to each uncertain parameter in the probabilistic calculations its best-estimate value (the mode or median of the PDF).

The main conclusions are summarized here.

a. The overall peak total risk is similar in the deterministic base case to that given by the probabilistic calculations.
b. In the time range 10^2 to 10^4 years, ^{129}I is the dominant contributor to risk, as in the probabilistic calculations.
c. ^{59}Ni hardly contributes at all to risk in the deterministic base case, indicating that its significant contribution to the mean risks arises from realizations with less than average return time of this radionuclide to the biosphere.
d. Removal of the barrier provided by the ILW backfill was found to affect risk significantly; in the case of the ^{129}I contribution, this is mainly due to its effect on the spreading in time of the release to the geosphere, whereas for ^{59}Ni it is associated with the change in travel time affecting the amount of decay.
e. Decreasing the barrier thickness would increase risks, to an extent intermediate between the base case and the variant with zero thickness; increasing the barrier thickness, however, is unlikely to reduce risks significantly relative to the base case.
f. Decreased groundwater travel times in the geosphere leads to a significant increase in risk; in the case of the ^{129}I contribution, this is mainly due to the associated reduction in the spreading in time of the arrival in the biosphere, whereas for ^{59}Ni, the effect is because reduced travel times allow less decay to occur.
g. The variants involving either an increased flux of groundwater through the repository, or changes to near-field chemistry, do not lead to very great increases of risk relative to the base case.

REFERENCES

1. Agg, P. J., et al., P-KAERI 94 Performance and Environmental Assessment of a Radioactive Waste Repository in Korea, NEMAC/AEA Technology, 1995.

2. Park, H. S., et al., A Study on the Requirements for Basic Design of a Repository for Low-Level Radioactive Waste, KAERI-NEMAC/PR-32/93, 1994.

3. Brown, P. L., et al., HARPHRQ: A Geochemical Speciation Program Based on PHREEQE, NSS/R188, UK Nirex, 1991.

4. Cross, J. E., et al., HATCHES - A Thermodynamic Database and Management System, NSS/R212, UK Nirex, 1990.

5. Martin, J. S., et al., User Guide for BIOS-3A, NRPB-M285, NRPB, 1991.

6. Sinclair, J. E., et al., MASCOT and MOP Programs for Probabilistic Safety Assessment, NSS/R336, UK Nirex, 1994.